Iran University of Science and Technology

International Journal of

Railway Research

ISSN: 2423-3838

Pitting growth detection in the gear transmission system of a locomotive using statistical features

Mohammad Ali Rezvani[1*], Farshad Niksai[1]

[1]School of Railway Engineering, Iran University of Science and Technology, Tehran, Iran.

ARTICLE INFO

Article history:
Received: 1.03.2024
Accepted: 5.07.2024
Published: 7.07.2024

Keywords:
Locomotive power transmission system
Gear defects
Pitting growth
Field observations
Failure statistics

A B S T R A C T

Failure of gears in locomotive power transmission system causes interruption in service and may lead to derailment or other train related disasters. This creates a drastic problem with the trustiness of the operations. Therefore, for the sake of safe and cost-effective operations early detection of failures including gear faults is of great importance. The purpose of this research is to explor the possibility of early detection of gear pitting in locomotive poower transmission system. For this purpose, the dynamic response of the gear system with pitting defects in different scenarios is scrutenized. The primary excitation to the gear dynamic system comes from the time-variant mesh stiffness. The effect of pitting growth on the potential energy of the system in different scenarios is analytically estimated. Responses in time and frequency domains are examined. Some statistical features are used. Features most sensitive to the failure that enable the detection of gear tooth pitting and its propagation are introduced. The theoretical results are compared and validated with a laboratory test setup. It is also endeavored to uncover the earliest possible level at which the removed surface can be detected. Hence the effect of the pitting growth due to geometric parameters such as the radius of pitting, number of pits, and number of teeth with pits are examined.

1. Introduction

Locomotives are multifaceted machines, with many critical components. Considering the wide usage of gears in power transmission systems, it points to the great benefit of monitoring and studying these machineries. The gear systems are used with the intent for reaching constant transmission ratio, high reliability, and high efficiency [1]. However, various gear faults can occur due to depraved working conditions such as exposure to heavy loads, and high fatigue [2]. The gear defects cause 60% of gearbox failures [3]. The most materialized failures are tooth cracks, tooth surface pitting, and tooth breakage [3].

Failures of gears have been identified by maintenance experts in field operations. In the presence of failure, the vibrational performance of the vehicle detracts. Failure occurrence causes discontinuity in transmission and can lead to derailment or other train-related disasters. This creates a drastic problem with the trustiness of the train task. Therefore, for the sake of safe and cost-effective train operation, early failure detection is of great importance.

However, scrutinizing the gear transmission system of locomotives and their dynamic performance have not been of prime importance to the researchers.

Meanwhile, dynamics of gear systems and their time-varying mesh stiffness for healthy and defective gears, based on vibration analysis, have attracted considerable attention.

*Corresponding author
Email: rezvani_ma@iust.ac.ir

[DOI: 10.22068/ijrare.342]

Several reports focused on the vibrational motion of defective gears and suggested different models. These models varied by their degrees of freedom. The researchers discussed the simplest models with one degree of freedom and continued to the complex multi-degrees of freedom models. Modeling of the mesh stiffness is also of prominence [4]. The models differ depending on the consideration of torsional motion with or without coupling with longitudinal motion. Bartholomeus introduced a model with 8 degrees of freedom [5]. Feng and Zhao [6] reported a planetary gearbox and proposed a mathematical model for inquiring about the pitting failure, using frequency modulation and amplitudes. However, their model couldn't simulate the pitting progress. Also, making the connection between the physical components of the gearbox and the model should be noticed. Chaari *et al.* [7], Zhe *et al.* [8], and Abu El-Seoud *et al.* [9], worked on pitting and modeled it as rectangular. Chaari *et al.* [10] and Choy *et al.* [11] tried to correct the shape of the pit. However, there isn't any relationship between pitting growth and time-variant mesh stiffness in their study.

Many researchers used potential energy to specify the mesh stiffness and vibration displacement for faulty teeth [11].

Most studies have concentrated on the occurrence of just one failure on one tooth. Although lately, limited research has modeled multiple faults on multiple teeth [12]. Rezaei *et al.* [13] studied detecting multi-crack in helical gear teeth making use of the transmission error ratio. Several pits on multiple teeth modeled in a circular shape, have been simulated by Liang *et al.* [14]. He used potential energy for mesh stiffness assessment. Hou *et al.* studied the effect of pitting on vibration response and mesh stiffness [15]. Thunuguntla *et al.* probed the effect of pitting damage in a spur gear through finite element modeling [16]. Grzeszkowski *et al.* classified pitting damage using vibration measurement [17].

Recently some researchers considered multiple faults and coexisting damage on a gear [18-19]. Niksai and Rezvani modeled pitting and chipping faults concurrently [20]. Ouyang *et al.* diagnosed and analyzed pitting-crack coupling faults [21].

Considering the importance of the safety and accessibility of the locomotives it is important to identify pitting propagation. Detecting pitting propagation is the main purpose of the present research. The simulation and determination of the amount of damage to the gear need to be as fast as possible. It would then result in higher dynamic efficiency. Pinion failures are costly, and the broken pinion can cause troubles such as the derailment of the locomotive and endangering safety of railway transportation.

The present research also endeavors to uncover the earliest possible level at which the removed surface can be detected. Hence the effect of the pitting growth due to geometric parameters like the radius of pitting, number of pitting, and number of teeth with pits are examined.

To serve this purpose, a speculative model for the locomotive transmission system is provided. It considers longitudinal and torsional oscillations and the flexibility of the system components. Rail irregularities are ignored, and the system's running speed is constant. The theory of potential energy is used to calculate the time-varying mesh stiffness. System vibration response is used to calculate some relevant statistical features [4]. While providing valuable data, this can lead to proper results in fault detection [22]. Within this subject, various statistical indicators were suggested [23-24].

Moreover, an experimental rig setup replicating a scaled locomotive power transmission arrangement is assembled. This setup is then used for validating the outcome of the modeling process.

It needs to be noted that the field observations provided in this study are mostly focused on the cases of the presence of multi-pitting on a single tooth and multiple teeth in a gear. This scheme, to the knowledge of the authors, has not been previously used for the fault detection of locomotive transmission systems. The statistical features provided in this study are further discussed in the later sections of this manuscript. The variations in parametric studies are examined and the ones with the highest sensitivity are applied in the experimental setup for validation purposes.

2. Sculpting tooth pitting and mesh toughness assessment

2.1. Gear tooth failure

[DOI: 10.22068/ijrare.342]

Pitting takes place on the teeth of the gears due to metal-to-metal contact. Based on the visual inspection it was found that pitting has the highest percentage among all types of gear failure. Pitting growth may lead to severe damage and a reduction in train safety.

Figure 1 displays a real pitting defect in a pinion of a power transmission system of a locomotive at an early stage. Identification of this failure before the critical level is very important for the safety and accessibility of locomotives. Theoretically, pitting cases are numerous. Encompassing a wide range of defects, such as changes in the radius of each pit, the number of pits on each tooth, and the number of faulty teeth.

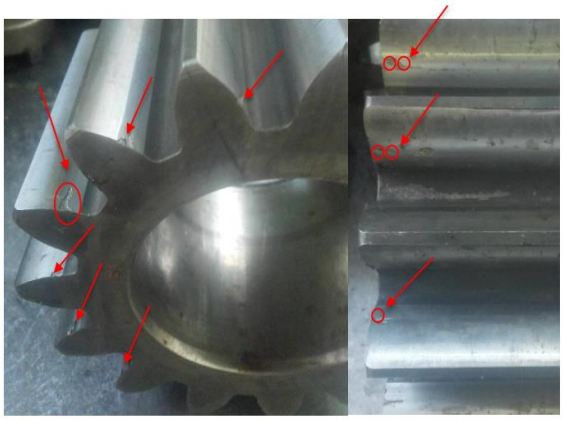

Fig. 1. Real pitting in a gear power transmission system of a locomotive

Pitting can be reproduced in a different number of teeth. In this study, more realistic mathematical modeling of pitting is considered. A variety of six defective cases are considered.

Table 1. Defect types and specifics of one tooth

Case No.	No. of pitted teeth	No. of pits on each tooth	Removed surface (%)
1	1	1	0.5
2	3	1	1.5
3	6	1	3.1
4	1	6	3.1
5	3	6	9.4
6	6	6	18.8

The details of the different failure cases concerning the actual sizes of defects are presented in Table 1.

Due to the geometry of the pits on the pinion's surface, the pit radius and depth are assumed to be 2 mm and 0.5 mm, respectively. Detection of these pits is the main purpose of the simulation procedures. Determination of the amount of damage on a gear, as soon as possible, would then result in longer gearbox life and higher dynamic proficiency.

2.2. Assessing mesh stiffness

Many reports were interested in calculating mesh stiffness for pitting based on potential energy exclusively. Tian *et al.* computed mesh stiffness for chipping and Liang *et al.* did the same for pitting [14,25]. The tooth was shaped like a girder beam. The Hertzian, shear, axial, and bending stiffnesses are used to estimate the intact cumulative energy in the meshing tooth pair. The tooth profile is modeled with involute profiles, regarding the teeth contours of the corresponding gear set. The production and transmission errors are neglected. Lubrication is assumed to be ideal. The gear nucleus is deemed rigid, whereas the teeth are pliable. Such a strategy was used in multiple research projects in this field.

Figure 2 presents a schematic of multiple pits on the tooth surface. For the simplicity of the modeling, the gear tooth fillet contour is represented by a straight line. (u, r, δ) indicate the pitting on the tooth plane. δ is the pitting depth, r is the radius of the pit circle and u is the interval between the pit center and the root. The pitting influences the shear ks, bending kb, and compressive ka stiffnesses and can be estimated by using the following equations, [26].

Where E and υ represent Young's modulus and Poisson's ratio. L is the width of the teeth. Z and N are the number of teeth and pits respectively. F represents the pressure angle; and is decomposed into its components. The angle between the action line and the horizontal line is β_F.

[DOI: 10.22068/ijrare.342]

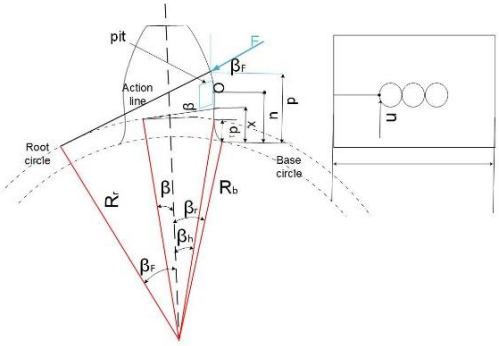

Fig. 2. Multiple pitting failure [23]

Half of the tooth angle on the base and the root circles are denoted with β_h and β_r. *ΔL_xj, ΔI_xj,* and *ΔA_xj* (for the jth pitting), are the reduction of the tooth contact width, inertia and area of the tooth section. The distance to the touch base point is *x*. *ΔL_xj, ΔI_xj,* and *ΔA_xj* are according to the following equations.

$$\Delta L_x = \begin{cases} 2\sqrt{r^2-(u-x)^2} & x \in [u-r\,,u+r] \\ 0 \end{cases} \quad (1)$$

$$\Delta A_x = \begin{cases} \Delta L_x \delta & x \in [u-r\,,u+r] \\ 0 \end{cases} \quad (2)$$

$$\Delta I_x = \begin{cases} \frac{1}{12}\Delta L_x \delta^3 + \frac{A_x \Delta A_x \left(h_x - \delta/2\right)^2}{A_x - \Delta A_x} \\ 0 \end{cases} \quad (3)$$

$$x \in [u-r, u+r]$$

Following Yang's research, for a paired tooth, linearization to a constant along the whole action line for the Hertz stiffness is used [26]:

$$k_h = \frac{\pi E (L_{eff})}{4(1-\upsilon^2)} \quad (4)$$

For pitting L_{eff} is defined as follows [14]:

$$L_{eff} = \begin{cases} L, & otherwise \\ L - 2\sqrt{r^2-(u-x)^2}, & u-r < x < u+r \end{cases} \quad (5)$$

In a pair of gears one or two pairs of teeth engage with a contact ratio of one or two. For single-tooth-pair engagement the total mesh stiffness is [26]:

$$K_t = \frac{1}{\frac{1}{k_h}+\frac{1}{k_{b1}}+\frac{1}{k_{s1}}+\frac{1}{k_{a1}}+\frac{1}{k_{b2}}+\frac{1}{k_{s2}}+\frac{1}{k_{a2}}} \quad (6)$$

$$k_t = k_{t_1} + k_{t_2} \quad (7)$$

$$= \sum_{i=1}^{2} \frac{1}{\frac{1}{k_{h,i}}+\frac{1}{k_{b1,i}}+\frac{1}{k_{s1,i}}+\frac{1}{k_{a1,i}}+\frac{1}{k_{b2,i}}+\frac{1}{k_{s2,i}}+\frac{1}{k_{a2,i}}} \quad (8)$$

The indices *1* and *2* refer to the driving and driven gears. *i* is for the corresponding paired teeth.

$$\frac{1}{k_b} = \frac{[1-\frac{(Z-2.5)\cos\beta_F \cos\beta_r}{Z\cos\beta_p}]^3 - (1-\cos\beta_F\cos\beta_h)^3}{2EL\cos\beta_F \sin^3\beta_h} + \int_{-\beta_F}^{\beta_h} \frac{3\{1+\cos\beta_F[(\beta_h-\beta)\sin\beta-\cos\beta]\}^2(\beta_h-\beta)\cos\beta}{E(2L[\sin\beta+(\beta_h-\beta)\cos\beta]^3 - 3\sum_1^N \frac{\Delta I_{xj}}{R_b{}^3})}\, d_\beta \quad (9)$$

$$\frac{1}{k_s} = \frac{1.2(1+\upsilon)\cos^2\beta_F\,(\cos\beta_h - \frac{Z-2.5}{Z\cos\beta_p}\cos\beta_r)}{EL\sin\beta_h} + \int_{-\beta_F}^{\beta_h} \frac{1.2(1+\upsilon)\,(\beta_h-\beta)\cos\beta\cos^2\beta_F}{E(L[\sin\beta+(\beta_h-\beta)\cos\beta] - 0.5\sum_1^N \frac{\Delta A_{xj}}{R_b})}\, d_\beta \quad (10)$$

$$\frac{1}{k_a} = \frac{\sin^2\beta_F\,(\cos\beta_h - \frac{Z-2.5}{Z\cos\beta_p}\cos\beta_r)}{EL\sin\alpha_h} + \int_{-\beta_{F,i}}^{\beta_h} \frac{(\beta_h-\beta)\,\cos\beta\,sin^2\beta_F}{E(2L[\sin\beta+(\beta_h-\beta)\cos\beta] - \sum_1^N \frac{\Delta A_{xj}}{R_b})}\, d_\beta \quad (11)$$

3. Locomotive power transmission system

3.1. The model

The system of interest holds a single-stage gearbox. Eight degrees of freedom is used to present the torsional and longitudinal motions. All related components are considered. Axle and rotor are assumed to be flexible. Masses and moments of inertia of the system components are figured via SolidWorks engineering software. The specifics of the gear are presented in Table 2.

The dynamic model is illustrated schematically, in Fig. 3. *Tm* is the torque that drives the traction motor. The resistance torque is presented with *Tw*. The driver and driven

[DOI: 10.22068/ijrare.342]

shafts are assumed to be flexible. All components of the system are ideally lubricated and in perfect physical condition. The physical influence of rail irregularities is neglected.

Table 2. The specifics of the gear

Property	Pinion (driving)	Gear (driven)
Number of teeth	60	17
Module (mm)	11.3	11.3
Angle of attack	20	20
Mass (kg)	192	21
Face width (mm)	123	123
Young's modulus (GPa)	206	206
Poisson's ratio	0.3	0.3

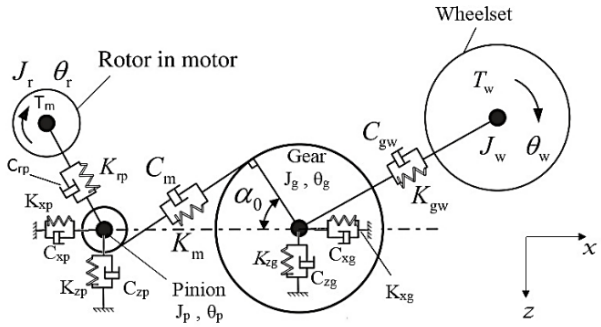

Fig. 3. The idealized gear model [27]

The system input and output shafts are considered as flexible. The analogous motion equations are elucidated in [28].

3.2. Numerical analysis

For the assessment of the system specifics based on the above sets of equations, a numerical analysis needs to be performed. Therefore, it is required to simulate the displacement signals of the pinion.

The proportion of damping to stiffness for the gear mesh is constant and is equal to 0.07 [29]. The gear set angular velocity and torque are based on a constant speed of travel at 60 km/h.

The torque exerted on the rotor by the traction motor that can provide 6 KNm is 1.7 kNm. The pinion rotation is at18.7 Hz, and meshing gears frequency is 317.9 Hz. The MATLAB software is used to solve the system motion equations.

4. Discussion of the results

4.1. Mesh stiffness reduction

As explained earlier, six different cases are defined to cover a wide range of gear pitting defects. The system equations are solved and for each case the mesh stiffness of the paired teeth is assessed.

As the fault grows, it is observed that the mesh stiffness within the tooth interlacement period also reduces. Equation (12) is used for the assessment of the reduction of mesh stiffness.

The distinctions in mesh stiffness of the fit and flawed gear at the same angular translation are calculated by using Eq. (12). The results are presented in Table 3.

$$\delta_{k_t} = \left(\left| \sum_{f=1}^{F} \frac{k_{t1s}}{F} - \sum_{h=1}^{H} \frac{k_{t2m}}{H} \right| / \sum_{h=1}^{H} \frac{k_{t2m}}{H} \right) * 100\% \qquad (12)$$

K_{t1} is the mesh stiffness of a defective gear and k_{t2} is for the mesh stiffness of a perfect gear. F and H are for the estimated mesh stiffness of a defected and a flawless gear, respectively.

Table 3. Averaged mesh stiffness reduction (%) caused by teeth engagements

Mesh period No.	single-tooth-pair interlacing period					
	case 1	case 2	case 3	case 4	case 5	case 6
1	0.49	0.49	0.49	6.26	6.26	6.26
2	0	0.48	0.48	0	6.02	6.02
3	0	0.47	0.47	0	5.99	5.99
4	0	0	0.47	0	0	5.96
5	0	0	0.47	0	0	5.91
6	0	0	0.46	0	0	5.84
	Double-tooth-pair interlacing period					
1	0.01	0.01	0.01	0.13	0.13	0.13
2	0	0	0.01	0.05	0	0.05
3	0	0	0.01	0.05	0	0.05
4	0	0	0.01	0	0	0.06
5	0	0	0.01	0	0	0.06
6	0	0	0.01	0	0	0.07

4.2. Oscillatory behavior

Figure 4 exhibits the calculated vibrational signal for the six pre-defined defected gear scenarios. The results are for two complete pinion rotations with a period of 0.1 seconds.

[DOI: 10.22068/ijrare.342]

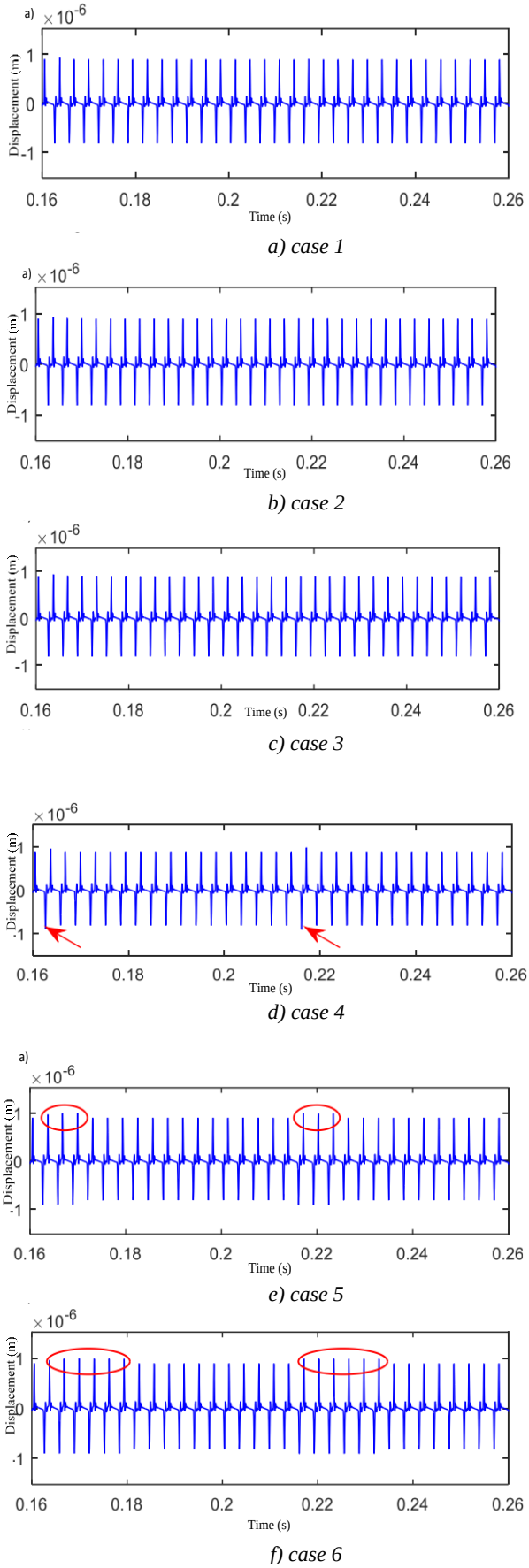

a) case 1

b) case 2

c) case 3

d) case 4

e) case 5

f) case 6

Fig. 4. The estimated faulty pinion displacements

Since the pinion in this gearset holds 17 teeth, one full revolution of the set endures 17 tooth contacts. Therefore, there will be 34 peaks present in two full-pinion revolutions. For flawless gear, the scale of the mounts is the same due to the teeth being in the same condition. The study continues with conniving the vibrational behavior of pinion for the defected cases. Obviously, for the defective pinions the amplitude of vibrations due to contacts do not stay the same and behave variably depending on the conditions of contact.

Translation response of the pinion in the vertical (*z*) direction for the defected gears is presented in Fig. 4. The defects descend from slight to severe Pits, respectively. For defect type 1, with the corresponding field observations provided in Table 1, the defected area is very small and the consequent fault symptoms in Fig. 4(a) are very weak. However, careful observation in Figs. 4(d) to (f) display one or multiple spikes (pointed to by circles or arrows) that are slightly higher signals. Fig. 4(a) displays the displacement described above for pitting scenario No. 1. This case holds 1 pit with a pitted area of 0.5%.

The small differences between the amplitude peaks are reasonable due to the heavy masses of the gears. In this case, the time domain signals would not be suitable for revealing the faults. Hence, other scrutiny methods are needed for detecting flaws in such circumstances. The use of some statistical revelation methods will be helpful. It is then decided to switch to practicing the use of some selected statistical features for validation purposes.

4.3. Tracing the failure using statistical features

As depicted in the previous section, revealing the level of pitting in different cases cannot be accomplished by merely resorting to gear vibration amplitudes. Some further processing of the gear response is deemed necessary. Therefore, the research continued by estimating some statistical features for portraying the behavior of the selected cases. To this end, the statistical indicators of vibrational signals are calculated for the faulty cases and compared with their healthy states. It is valuable to comprehend how the different levels of pitting growth affect the conforming statistical

[DOI: 10.22068/ijrare.342]

parameters. The following equation is used for comprehending the change in statistical index.

$$growth\ rate = \frac{F_i - F_0}{F_0} * 100\% \quad (13)$$

F_0 stands for the statistical parameter of a healthy state and F_i represents the ith failure. The thirty statistical features that are used frequently in most research, are calculated for the signals of displacement [23]. Then due to the sensitivity of features and how they change during fault growth, it was decided which one displays the most sensitivity. The selected statistical features include the Minimum, Maximum, Mean, Crest Factor, Clearance Factor, M6A and M8A indices for the displacement signal of the gear. Some of the useful features are presented in Eqns. (14&15) [23].

$$\frac{\frac{1}{N}\sum_{n=1}^{N}(d(n)-\bar{d})^6}{\left(\frac{1}{N}\sum_{n=1}^{N}(d(n)-\bar{d})^2\right)^3} \equiv M6A \quad (14)$$

$$\frac{\frac{1}{N}\sum_{n=1}^{N}(d(n)-\bar{d})^8}{\left(\frac{1}{N}\sum_{n=1}^{N}(d(n)-\bar{d})^2\right)^2} \equiv M8A \quad (15)$$

Where the raw signal and the difference signal are presented with $x(n)$ and $d(n)$, respectively. The bar is for averaging.

The time and frequency domain data for the variations in the most influential statistical indicators of faulty cases are displayed in Figs. 5 and 6.

From data in Fig. 5(a), it is observable that the selected statistical features exhibit progressively increasing growth measures. Cases 1 and 2 are hardly distinguishable due to the tiny amount of removed surfaces. For defective cases 3 to 6, the differences in the estimated parameters are apparent. The fourth order central moment and variance with 20% and 10% changes for case 6 exhibit the highest and the second highest sensitivity, respectively.

It should be noted that variations of some indicators in the time domain (Fig. 5 (b)) versus increasing severity of the defect types have negative slopes. The behavior of the statistical indicators that have steadily declined is also presented.

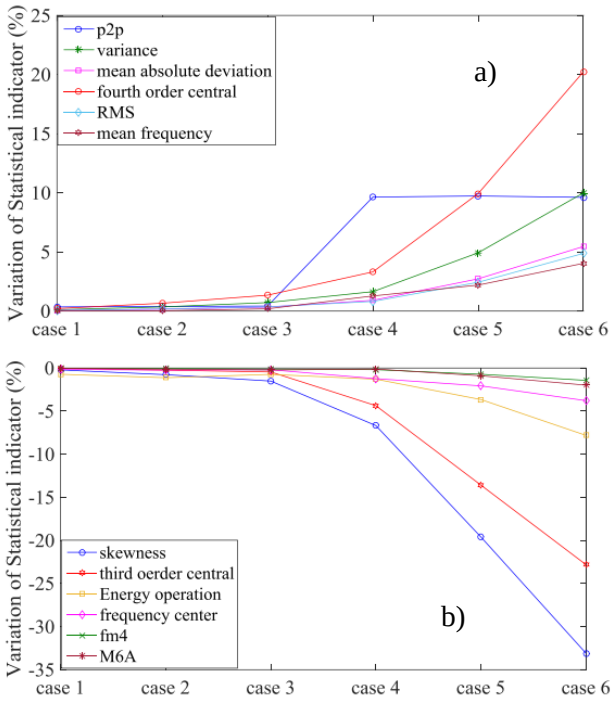

Fig. 5. Time-domain variations of the selected indices for the set of defective gears

The statistical indicator skewness with -30% variation exposed the most sensitivity in failure case number 6. Among these indicators, fourth order central moment and skewness have the best capability for pitting fault detections in the time domain.

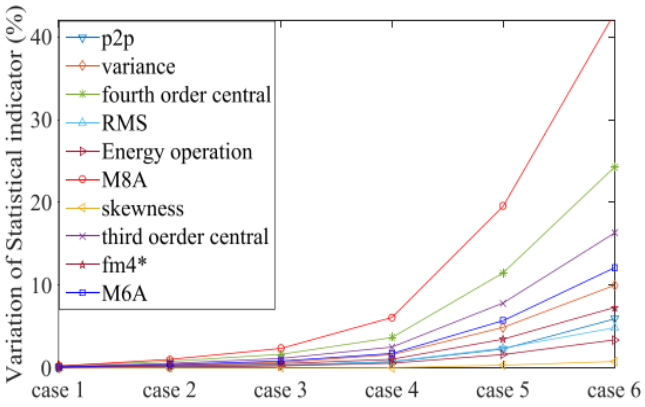

Fig. 6. Frequency-domain variations of the selected indices for the set of defective gears

In Fig. 6, the variation of statistical indicators in the frequency domain is presented. It is observed that the amplitudes of the indicators will increase gradually as the pitted area propagates in the pitted tooth (defect types become more severe). The statistical variations are clearer in the frequency domain. M8A and fourth order central indicators for fault detection exhibit the best performances in the frequency domain.

[DOI: 10.22068/ijrare.342]

5. The test rig

To evaluate the vibrational behavior of faulty gear cases, an experimental setup is prepared, Fig. 7. This setup is a scaled version of the real size locomotive power transmission system. The corresponding scale factor is one to five. The idea is to examine the sensitivity of the selected statistical indicators that are used for gear fault identification.

The test setup consists of a pair of gears, an electric motor with 2.2 KW of power, and a braking system consisting of a spring and rope. The scaled test rig represents the original gear mechanism. The pinion shaft delivers power to the main gear and the follower shaft. Spring and rope are used to exert brake torque on the follower shaft. A tachometer is used to count for the rotational speed of the shaft.

An accelerometer (CA-YD-189) is used to measure the system vibration signal at bearing pedestal near the pinion. The accelerometer sensitivity is 1000 mv/g. A data logger (Avant-7016) is used for data storage. The pinion rotational speed is the same as in the theoretical estimates (18.7 Hz). The brake torque exerted to the follower shaft through the spring and rope is equal to 14 Nm.

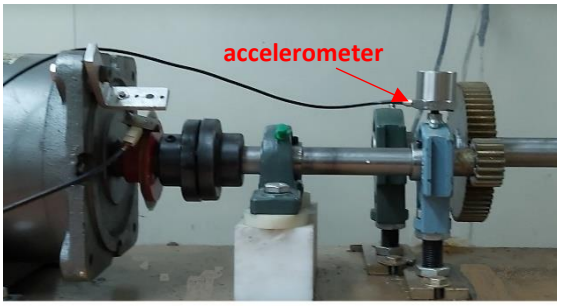

Fig. 7. A scaled (1/5) replica of the locomotive power transmission system

The scaled model is made of steel-vcn200 that is of the same material as in the real system.

The sampling frequency is set at 6 KHz. For different levels of gear fault growth, the vibrational signals are collected. The designated faulty pitted gears are provided by drilling multiple circular holes on the tooth surface, while the scale of the actual pits is served, Fig. 8. Only four pitted pinions are presented on Fig. 8 since defective pinions for cases 3 and 6 hold too many damaged teeth to be able to present them in a single picture.

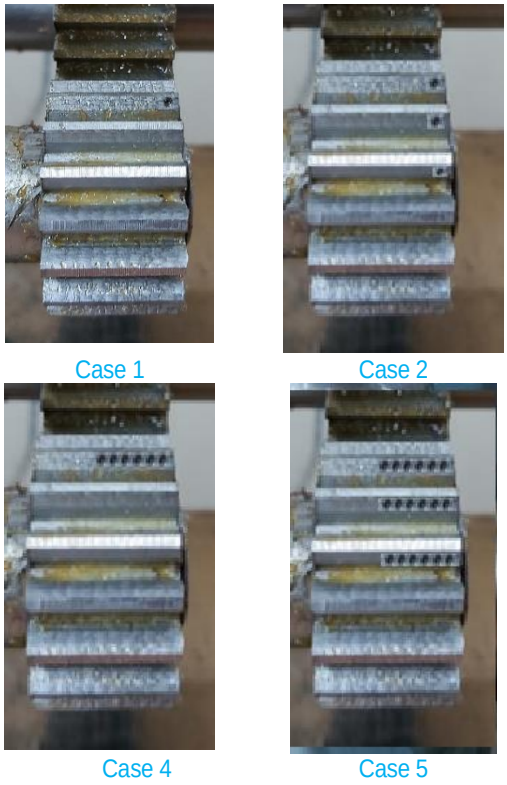

Fig. 8. Damaged pinions used for test purposes

The initial tests are performed with a flawless pinion. This is followed by mounting faulty gears and taking several measurements.

The designated statistical indicators for all measurements are estimated. Time-domain and frequency-domain observations are used. The pitting defect progression for separate circumstances are assessed and linked.

The variation between featured indicators for the flawless and defected pinions are identified as the defect growth rate.

The statistical indicators that present the best performance in fault identification (the larger change regarding the different fault scenarios) are compared with the test results. The compatibility between the estimated and the measured results indicated the ability to identify the damaged gears through measurements. Some sample results are presented on Fig. 9.

The accuracy of the accelerometer used for the measurements is 1000 mv/g. The measured signals are checked to make sure that there is no damaging interference between the recorded

[DOI: 10.22068/ijrare.342]

signal and the accelerometer measurement limits.

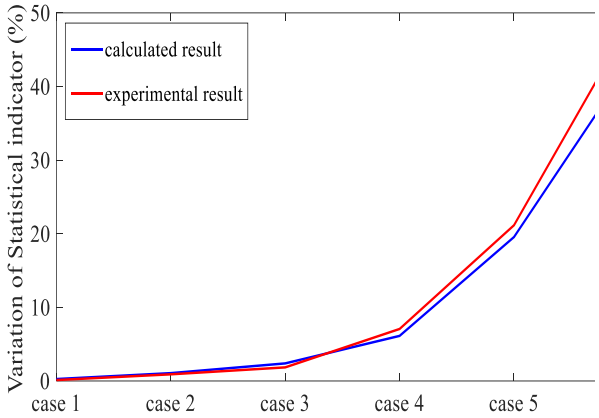

Fig. 9. Variations in the M8A indicator for the estimated and measured signals

6. Conclusions

This research presented an analytical model to estimate the effects of pitting growth in a gearbox. The subject of interest was a selected locomotive power transmission system. The influence of the defect appeared in the mesh stiffness estimations for the flawless, as well as, the defective gears. Time-dependent estimations are used. A total of six defective cases were examined. The vibrational response of these six cases was analyzed. The first three defective cases hold one, three, and six damaged teeth, respectively, while each tooth contains one representative pit per tooth in genuine dimensions. In those cases, due to the geometry of the gear, variations sighted in the vibration response were small. Then, to demonstrate growth in the pitted section, six pits were drilled on one, three, and six teeth on the next set of test pinions. Changes in the estimated displacement signals were well observed. An experimental setup is also prepared for the verification of theoretical predictions. Some statistical indicators are used for comparisons. The subsequent results are obtained:

- For test cases 1 and 2, the variation in statistical indicators is small (<2%). Then the defects are hardly identifiable. This is due to the small level of the removed surface compared to pinion geometry.
- If defects take place on several teeth concurrently, like in case 3 with one pit on 6 teeth, the variation of M8a growth is about 2 folds. This can be easily detected in the frequency domain calculations.
- The variations in the statistical indicators in the time domain concerning the damage propagation are categorized into two groups. The ones with a positive slope, among which the fourth-order central moment displays the most sensitivity with 20 percent change between different scenarios, and the ones with a negative slope, in which skewness displays the most sensitivity with 34 percent variation.
- In the frequency domain, the growth in statistical indicators is observed to have a positive size and slope. Among these M8A with a 42 percent variation exhibits the most sensitivity.
- In the frequency domain, variations of statistical indicators are more apparent than in the time domain. Propagations in damage responded with more uniform behavior. Thus, utilizing the statistical indicators in the frequency domain is the preferred pitting identifier procedure.

The outcome from the experimental setup demonstrates that indicator M8A exhibits an adequate agreement with the theoretical findings.

References

[1] Z. Chen, W. Zhai, and K. Wang, Dynamic investigation of a locomotive with effect of gear transmissions under tractive conditions. Journal of Sound and Vibration, 408 (2017) 220-233.

[2] Z. Chen, and Y. Shao, Dynamic simulation of spur gear with tooth root crack propagating along tooth width and crack depth. Engineering Failure Analysis. 18(8) (2011) p. 2149-2164.

[3] L. Gelman, R. Zimroz, J. Birkel, H. Leigh-Firbank, D.M. Simms, B. Waterland, and G. Whitehurst, Adaptive vibration condition monitoring technology for local tooth damage in gearboxes. Journal of Non-Destructive

[DOI: 10.22068/ijrare.342]

Testing and Condition Monitoring, 47(8) (2005) p. 461-464.

[4] I. Howard, S. Jia, and J. Wang, The dynamic modelling of a spur gear in mesh including friction and a crack. Mechanical Systems and Signal Processing. 15(5) (2001) p. 831-853.

[5] W. Bartelmus, Mathematical modelling and computer simulations as an aid to gearbox diagnostics. Mechanical Systems and Signal Processing,15(5) (2001) p. 855-871.

[6] Z. Feng, and M.J. Zuo, Vibration signal models for fault diagnosis of planetary gearboxes. Journal of Sound and Vibration, 331(22): (2012) p. 4919-4939.

[7] F. Chaari, W. Baccar, M.S. Abbes, and M. Haddar, Effect of spalling or tooth breakage on gear mesh stiffness and dynamic response of a one-stage spur gear transmission. European Journal of Mechanics-A/Solids, 27(4) (2008) 691-705.

[8] C. Zhe, H. Niaoqing, G. Fengshou and Q. Guojun, Pitting damage levels estimation for planetary gear sets based on model simulation and grey relational analysis. Transactions of the Canadian Society for Mechanical Engineering, 35(3) (2011) 403-417.

[9] S.A. Abouel-seoud, E.S. Dyab and M.S. Elmorsy, Influence of tooth pitting and cracking on gear meshing stiffness and dynamic response of wind turbine gearbox. Int. J. Sci. Adv. Technol, 2(3) (2012) 151-165.

[10] F. Chaari, T. Fakhfakh and M. Haddar, Dynamic analysis of a planetary gear failure caused by tooth pitting and cracking. Journal of Failure Analysis and Prevention, (6) 2 (2006) 73-78.

[11] F.K. Choy, V. Polyshchuk, J.J. Zakrajsek, Analysis of the effects of surface pitting and wear on the vibration of a gear transmission system. Tribology International, 29(1): (1996) p. 77-83.

[12] H. Ma, Z. Li, M. Feng, R. Feng, and B. Wen, Time-varying mesh stiffness calculation of spur gears with spalling defect. Engineering Failure Analysis, 66, (2016) 166-176.

[13] M. Rezaei, M. Poursina, S.H. Jazi and F.H. Aboutalebi, Multi crack detection in helical gear teeth using transmission error ratio. Journal of Mechanical Science and Technology, 33(3), (2019) 1115-1121.

[14] X. Liang, H. Zhang, L. Liu and M. J. Zuo, The influence of tooth pitting on the mesh stiffness of a pair of external spur gears. Mechanism and Machine Theory, (2016),106, 1-15.

[15] J. Hou, S. Yang, Q. Li, Y. Liu, Effect of a novel tooth pitting model on mesh stiffness and vibration response of spur Gear. Mathematical Method and Application of Machine Learning. (2022)

[16] SG. Thunuguntla, A. Hood, C. Cooley, Tooth mesh characterization of spur gear pairs with surface pitting damage, SAE Technical Paper (2023)

[17] M. Grzeszkowski, S. Nowoisky, P. Scholzen, G. Kappmeyer, C. Gühmann, J. Brimmers, and C. Brecher, Classification of gear pitting damage using vibration measurements. tm-Technisches Messen 88, no. 5 (2021): 282-293.

[18] Happi, Kemajou Herbert Yakeu, Bernard Xavier Tchomeni Kouejou, and Alfayo Anyika Alugongo. Influence of coexistence of pitting and cracking faults on a two-stage spur gear system. Vibration 6.1 (2023): 195-217.

[19] Ren, Yulin, Guoyan Li, Xiong Li, Jingbin Zhang, Runjun Liu, and Sifan Shi, Compound fault characteristic analysis for fault diagnosis of a planetary gear train. Sensors 24, no. 3 (2024): 927.

[20] F. Niksai, M.A. Rezvani, Concurrent impact of chipping and pitting damages in a locomotive power transmission system. J Mech Sci Technol 36, (2022) 3791-3800.

[21] T. Ouyang, G. Wang, L. Cheng, J. Wang, Comprehensive diagnosis and analysis of spur gears with pitting-crack coupling faults. Mechanism and Machine Theory 176 (2022): 104968.

[22] X. Liang, M.J. Zuo and Z. Feng, Dynamic modeling of gearbox faults: A review. Mechanical Systems and Signal Processing, 98, (2018) 852-876.

[23] X. Zhao, M.J. Zuo and Z. Liu, Diagnosis of pitting damage levels of planet gears based on ordinal ranking. In 2011 IEEE Conference on Prognostics and Health Management (pp. 1-8). IEEE. (2011, June).

[24] Z. Liu, J. Qu, M.J. Zuo and H.B. Xu, Fault level diagnosis for planetary gearboxes using hybrid kernel feature selection and kernel Fisher discriminant

[DOI: 10.22068/ijrare.342]

analysis. The International Journal of Advanced Manufacturing Technology, 67(5-8) (2013)1217-1230.

[25] X. Tian, M.J. Zuo and K.R. Fyfe, Analysis of the vibration response of a gearbox with gear tooth faults. in ASME 2004 International Mechanical Engineering Congress and Exposition. American Society of Mechanical Engineers. (2004)

[26] D.C.H. Yang and Z.S. Sun, A Rotary Model for Spur Gear Dynamics, ASME Journal of Mechanisms, Transmissions, and Automation in Design, 107, PP. 529-535, 1985.

[27] Z. Chen, W. Zhai, and K. Wang, A locomotive–track coupled vertical dynamics model with gear transmissions. Vehicle System Dynamics, 55(2) (2017) 244-267.

[28] Kong, Yiyi, Hong Jiang, Ning Dong, Jun Shang, Pengfei Yu, Jun Li, Manhua Yu, and Lan Chen, Analysis of time-varying mesh stiffness and dynamic response of gear transmission system with pitting and cracking coupling faults. *Machines* 11, no. 4 (2023): 500.

[29] M. Amabili and A. Rivola, Dynamic analysis of spur gear pairs: steady-state response and stability of the SDOF model with time-varying meshing damping. Mechanical Systems and Signal Processing, 11(3), (1997), 375-390.

[DOI: 10.22068/ijrare.342]